Journal of Medicinal Chemistry

Article

Structure-Guided Discovery of Potent and Selective Inhibitors of ERK1/2 from a Modestly Active and Promiscuous Chemical Start Point

Richard A Ward, Paul A. Bethel, Calum Cook, Emma Davies, Judit É. Debreczeni, Gary Fairley, Lyman Feron, Vikki Flemington, Mark A. Graham, Ryan Greenwood, Nicola Griffin, Lyndsey Hanson, Philip Hopcroft, Tina D. Howard, Julian Hudson, Michael James, Clifford D. Jones, Christopher R Jones, Scott Lamont, Richard James Lewis, Nicola Lindsay, Karen Roberts, Iain Simpson, Steve St-Gallay, Steve Swallow, Jia Tang, Michael Tonge, Zhenhua Wang, and Baochang Zhai

J. Med. Chem., **Just Accepted Manuscript** • DOI: 10.1021/acs.jmedchem.7b00267 • Publication Date (Web): 04 Apr 2017

ACS Publications

Journal of Medicinal Chemistry is published by the American Chemical Society. 1155 Sixteenth Street N.W., Washington, DC 20036

Structure-Guided Discovery of Potent and Selective Inhibitors of ERK1/2 from a Modestly Active and Promiscuous Chemical Start Point

Richard A. Ward*[1], Paul Bethel[2], Calum Cook[1], Emma Davies[1], Judit E. Debreczeni[1], Gary Fairley[1], Lyman Feron[1], Vikki Flemington[1], Mark A. Graham[2], Ryan Greenwood[1], Nicola Griffin[3], Lyndsey Hanson[3], Philip Hopcroft[1], Tina D. Howard[1], Julian Hudson[1], Michael James[1], Clifford D. Jones[4], Christopher R. Jones[4], Scott Lamont[1], Richard Lewis[2], Nicola Lindsay[1], Karen Roberts[1], Iain Simpson[1], Steve St-Gallay[4], Steve Swallow[2], Jia Tang[5], Michael Tonge[1], Zhenhua Wang[5], Baochang Zhai[5].

[1]IMED Oncology and Discovery Sciences, AstraZeneca, Darwin Building, 310 Cambridge Science Park, Milton Rd, Cambridge, CB4 0WG and AstraZeneca, Hodgkin Building, c/o Darwin Building, 310 Cambridge Science Park, Milton Rd, Cambridge, CB4 0WG, UK. [2]AstraZeneca, Charter Way, Macclesfield, SK10 2NA, UK.

[3]AstraZeneca, Alderley Park, Macclesfield, SK10 4TG, UK.

[4] Former employee of AstraZeneca.

[5]Pharmaron Beijing Co., Ltd., 6 Taihe Road BDA, Beijing, 100176, P.R. China.

Keywords

ERK1/2; inhibitors; RAS/RAF/MEK/ERK signaling pathway; structure-based drug design; SBDD; oncology.

Abstract

There are a number of small molecule inhibitors targeting the RAS/RAF/MEK/ERK signaling pathway either approved or in clinical development for oncology across a range of disease indications. The inhibition of ERK1/2 is of significant current interest as cell lines with acquired resistance to BRAF and MEK inhibitors have been shown to maintain sensitivity to ERK1/2 inhibition in pre-clinical models. This manuscript reports on our recent work to identify novel, potent and selective reversible ERK1/2 inhibitors from a low molecular weight, modestly active and highly promiscuous chemical starting point **4**. To guide and inform the evolution of this series, inhibitor binding mode information from x-ray crystal structures was critical in the rapid exploration of this template to compound **35**, which was active when tested in *in vivo* anti tumour efficacy experiments.

Introduction

The MAPK (RAS/RAF/MEK/ERK) pathway plays a central role in controlling mammalian cell cycle progression, differentiation, protein synthesis, metabolism, survival, migration and senescence. This pathway is activated by a wide range of receptors, including receptor tyrosine kinases (RTKs), G protein-coupled receptors (GPCRs) and cytokine receptors, which results in the activation of the RAS family of GTPases (KRAS, NRAS and HRAS). Subsequently, signals are transmitted downstream through RAF (BRAF, CRAF, and ARAF) and MEK (MEK1 and MEK2) protein kinases. MEK1 and MEK2 are dual-specificity kinases that activate ERK1 and ERK2 via the phosphorylation of conserved threonine and tyrosine residues in the T-E-Y motif located within the activation loop. ERK1 and ERK2 control the output of the MAPK pathway by activating their many substrates, both nuclear and cytoplasmic[1, 2]. Direct phosphorylation of transcription factors induces extensive changes in gene expression which promote cell cycle progression and regulates negative feedback mechanisms. The activation of the MAPK pathway is also impacted by scaffold proteins such as kinase suppressor of RAS 1 (KSR1), which increase the efficiency of the interactions between the enzyme and substrate at each step. The high frequency of mutations resulting in constitutive activation of the MAPK pathway provides a strong rationale for pharmacologically inhibiting the pathway. Mutations in BRAF have been identified in melanoma (60%), thyroid (~50%) and colorectal (10%) tumours[3] whereas RAS genes are mutated in colorectal (50%), melanoma (20%) and pancreatic (90%) tumours. Small molecule inhibitors targeting BRAF and MEK have been developed and have subsequently been approved in multiple disease indications[4,5]. BRAF inhibitors such as vemurafenib and dabrafenib demonstrate dramatic regression of melanomas carrying the BRAF V600E mutation[6], whereas BRAF wild-type tumours are refractory. However, acquired resistance to BRAF inhibitors occurs in a significant subset of patients, primarily from genetic alterations resulting in MAPK pathway reactivation[7,8]. In melanoma, BRAF inhibitor monotherapy is now superseded by BRAF plus MEK inhibitor combinations[9,10], although acquired resistance resulting in patient relapse remains an issue. In addition, several selective and potent non-ATP-competitive allosteric MEK1/2 inhibitors have also been developed and assessed in multiple clinical trials, with trametinib having been approved by the U.S. FDA. Efficacy as single agent therapy has been reported with MEK inhibitors in clinical settings such as BRAF mutant melanoma and serous low grade ovarian cancer[10], however there is limited data on monotherapy responses in other settings.

The direct targeting of ERK1/2, the key signalling node of the MAPK pathway, may provide another therapeutic option in tumours with mutations in BRAF or RAS genes. Importantly, ERK1/2 inhibition may have clinical

utility in overcoming acquired resistance to RAF and MEK inhibitors where MAPK pathway reactivation has occurred, such as BRAF mutant melanoma. ERK1 and ERK2 are 85% identical by sequence (significantly higher in the ATP binding site) and share some, if not all, of their functions with reported inhibitors assumed active against both. A range of reversible ERK1/2 small molecule inhibitors have been disclosed, including compounds such as **1** (SCH772984)[11], **2** (BVD-523)[12] and **3** (GDC-0994)[13] (Figure 1). There are also a number of reported clinical and pre-clinical inhibitors without chemical structures revealed including inhibitors from Celgene[14], Novartis[15], Kura Oncology[16] and Eli Lilly[17]. In addition, we have reported a series of highly selective covalent ERK1/2 inhibitors[18] using structure-based drug design. However, some trials involving ERK1/2 inhibitors have recently been stopped or no longer recruiting participants[14,19]. Therefore the identification of high quality, potent and selective inhibitors of ERK1/2 remains of great interest within oncology drug discovery and this paper details our recent research efforts towards this aim.

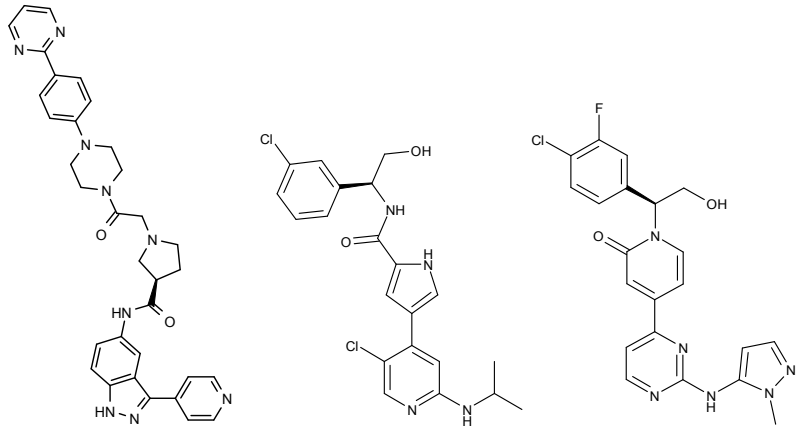

1 (SCH772984) **2** (BVD-523) **3** (GDC-0994)

Figure 1 – Selection of published ERK1/2 inhibitors.

Results and discussion

Series Identification. A number of hit identification approaches were considered in our efforts to identify high quality, potent and selective, reversible inhibitors of ERK1/2 with good physicochemical properties. In one approach we mined our historic kinase selectivity data from previous drug discovery projects to identify compounds with activity against ERK1 or ERK2. This analysis provided relatively few active compounds, however, a small number of hits were followed-up and tested in an ERK2 biochemical assay (run at 60 μM (K_M) ATP) to confirm and quantify the potency. Example **4**, with a pyrimidino-pyrrololactam core, appeared to be

the most interesting inhibitor with activity of 0.036 μM and relatively low molecular weight and Log *D* giving scope for further development (Table 1). Further testing of this compound included 1 mM ATP conditions in the biochemical assay to mimic cellular levels of ATP. In addition, a mechanism of action (MOA) cell assay measuring levels of phosphorylated ERK2 (pERK) and of the phosphorylation of the downstream kinase RSK (pRSK) in an A375 melanoma cell line, containing a $BRAF^{V600E}$ mutation. The active concentration of ERK2 used in the biochemical assays was determined by fitting compound inhibition data to the Morrison equation. This gave an active enzyme concentration of 0.6 nM and a tight-binding limit of 0.3 nM for both assays[20]. The drop-off due to increased ATP competition was calculated using the Cheng–Prusoff equation[21]. Based on our observed K_M of ERK for ATP (60 μM) and assuming that the compounds are fully competitive with ATP, we anticipated an 8.8-fold drop-off from the K_M ATP assay to the 1 mM ATP assay. The biochemical activity of **4** was consistent with ATP competitive behaviour, showing a drop-off of approximately 10-fold when using 1 mM ATP concentration. An additional observation however was the smaller than expected enzyme to cell drop-off, potentially this is due to off-target kinase activity as our previous work had indicated a significantly larger enzyme cell drop-off was expected for selective reversible ERK1/2 inhibitors. For example, **2** demonstrated high ATP biochemical activity <0.0003 μM, with pRSK MOA cell activity 0.14 μM[18]. To further characterise this risk the kinase selectivity profile (Eurofins Millipore assays) was generated and showed broad kinase activity, 75 out of a 128 kinase panel being inhibited > 80% at 1 μM compound concentration (Figure S1, supporting information). Whilst not conclusive, these results were supportive that off-target kinase activity might be contributing to the cellular activity of **4**. As we highlighted in our previous disclosure,[18] Eurofins assays for RAF and MEK1 are coupled assays, thereby compounds active in ERK1/2 may also appear active against RAF and MEK1. The MEK1 assay contains unactivated ERK2, with the CRAF assay containing unactivated MEK1 and ERK2. In-house biochemical testing was subsequently carried out to ensure these compounds were not active against MEK1. Apart from **4** (IC_{50} 1.9 μM versus MEK), all other compounds in this manuscript have IC_{50}'s >10 μM against MEK1.

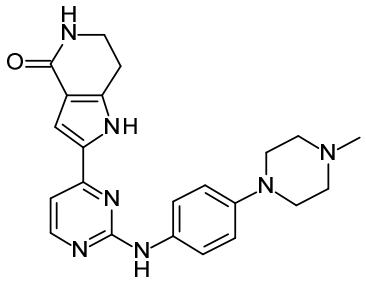

4

	4
ERK2 Biochemical, K_M ATP IC_{50} (μM)	0.036
ERK2 Biochemical, High ATP IC_{50} (μM)	0.37
Cell MOA A375 pERK/pRSK IC_{50} (μM)	0.16/0.57
Log $D_{7.4}$[a]	1.5
Aqueous Solubility (μM)[b]	189
Kinase Selectivity (N>80% out of 128 Kinase panel)	75

Table 1 – Profile of hit compound 4. All IC_{50} data are reported as μM and are the mean of at least n=3 independent measurements. [a]Distribution coefficient between 1-octanol and aqueous phosphate buffer at pH 7.4. [b]Solubility of compounds in aqueous phosphate buffer at pH 7.4 after 24 h at 25 °C (μM). Kinase selectivity data measured at 1 μM compound concentration.

Assessment of the binding mode of hit compound 4. In an effort to improve the potency and kinase selectivity of **4**, it was soaked in our ERK2 x-ray crystal structure system (Figure 1). The binding mode was successfully identified and showed the pyrimidine group formed a key interaction with the kinase hinge region (hydrogen bond to amide backbone of Met-108), with the amide group of the pyrrololactam interacting with the conserved salt bridge (Lys-54 and Glu-71). We had expected to observe an additional interaction of the carbonyl with a bound water molecule, consistent with the interaction observed in our covalent ERK1/2 inhibitors[18], however such a water molecule may not be visible at this resolution (2.74 Å). The anilino group interacted with the hinge region through a hydrogen bond donor to the backbone carbonyl of Met-108 and the piperidine group was directed into the 'solvent channel' of the kinase. In an effort to understand how to

improve ERK potency and selectivity the binding mode was compared to reported ERK1/2 inhibitors such as those by Aronov *et al*, illustrative example shown with (S)-4-(2-(2-chlorophenylamino)-5-methylpyrimidin-4-yl)-N-(2-hydroxy-1-phenylethyl)-1H-pyrrole-2-carboxamide (**5**)[22], figure 1. From this analysis we believed that we could improve potency and selectivity through both the modulation of the group positioned in the 'solvent channel' of the kinase and by extending our inhibitor into the glycine-rich loop region, contacting amino acids such as Tyr-36, Gly34 and Ile-56. Interestingly, without a group interacting in this region, Tyr-36 appears to fold back into the ATP pocket which appears to restrict access to the glycine-rich loop pocket, consistent with observations from Chaikuad *et al*[23]. It was also a concern to us that the direct interaction of the amide group of the pyrrololactam with the conserved salt bridge might be a negative influence on kinase selectivity. An additional interaction of compounds such as **5** reported by Aronov *et al* (and a number of other ERK1/2 inhibitors such as **2** and **3**) was a hydrogen bonding group, usually a hydroxyl, interacting with Asp-165 and Asn-152, offering the potential to improve potency whilst favourably modulating physicochemical properties.

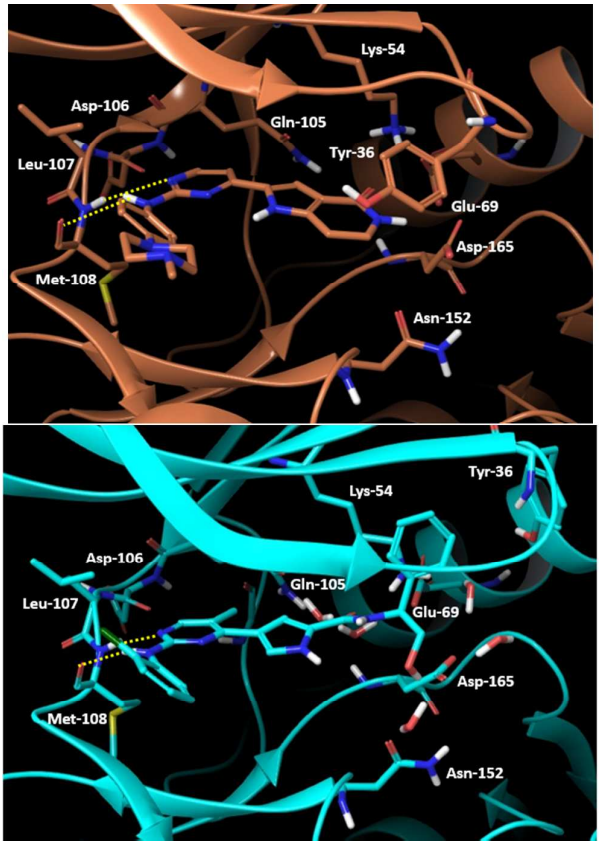

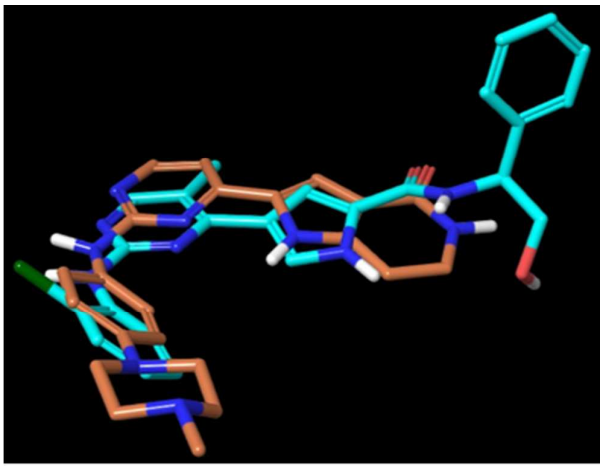

Figure 1 - Binding mode of **4** elucidated in human ERK2 crystal structure (top left, PDB Code 5NGU) published inhibitor **5** (middle, PDB Code 3I60) and overlaid inhibitors (bottom). All figures prepared using Maestro, version 2016-3 (Schrodinger).

It has previously been reported by Blake *et al* that the addition of a tetrahydropyran (THP) group in the solvent channel on an anilinopyrimidine core enhanced kinase selectivity, rationalised by the interaction with Lys-114[13,18]. **6** was synthesised to test if this hypothesis transferred to our identified pyrrololactam core (Table 2). The data generated was consistent in terms of demonstrating improved biochemical potency (IC_{50} 0.001 μM) and kinase selectivity (14/128 kinases with >80% inhibition at 1 μM). A decrease in terms of cellular activity (0.94 versus 0.57 μM in pRSK MOA assay) was observed but we rationalised this by the more selective nature of **6**, giving further evidence that off-target kinase activity contributed to the cellular activity of **4**.

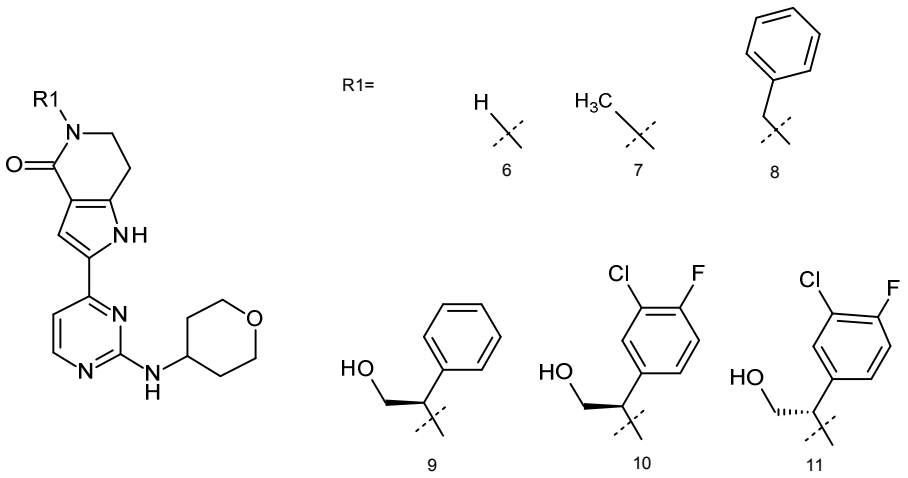

	6	7	8	9	10	11
ERK2 Biochemical, k_M ATP IC_{50} (μM)	0.0012	0.013	<0.00032	<0.00034	<0.00031	0.0011
ERK2 Biochemical, High ATP IC_{50} (μM)	0.0092	0.13	<0.0003	0.00043	0.00072	0.0037
Cell MOA A375 pERK/pRSK IC_{50} (μM)	0.96/0.94	>10/1.9	0.22/0.08	3.5/0.1	3.3/0.13	>30/0.25
Log $D_{7.4}$[a]	1.3	1.6	3.2	2.6	3.6	3.5
Aqueous Solubility (μM)[b]	760	98	<20	250	47	59
Kinase Selectivity (N>80% out of 128 Kinase panel)	14	ND	6	7	ND	ND
In-vitro Clearance HLM, (Rat Heps)[c]	<3 (<1)	9.7 (41)	55 (7.8)	36 (6.2)	73 (22)	99 (9)

Table 2 – Early SAR around pyrimidine-pyrololactam core. All IC_{50} data are reported as μM and are the mean of at least n=3 independent measurements. IC_{50} data reported as <0.0003 μM refers to values below the tight binding limit of the ERK2 biochemical assays. [a]Distribution coefficient between 1-octanol and aqueous phosphate buffer at pH 7.4. [b]Solubility of compounds in aqueous phosphate buffer at pH 7.4 after 24 h at 25 °C (μM). Kinase selectivity data measured at 1 μM compound concentration. [c]Human microsome (μL min^{-1} mg^{-1}) and rat hepatocytes metabolism intrinsic clearance (μL min^{-1} million $cells^{-1}$). ND, not determined.

Our next objective was to grow lead compound **6** into the glycine-rich loop to gain additional interactions to drive ERK1/2 potency and further improve kinase selectivity. From our structural overlays exemplified in figure 1 we believed it might be possible to achieve this through substitution of the lactam NH, a range of potential groups were subsequently assessed and prioritised using molecular modelling. To model such ideas the docking package Glide was used from Schrodinger (Maestro version 2016-3)[24] utilising in-house crystal structures prepared by the ligand and protein preparation protocols. **7** was synthesised to check if substitution was tolerated with a methyl group (0.013 μM compared for **7** to 0.0012 μM for **6**); although we saw a 10-fold decrease in potency the observation encouraged us to add larger groups that may fill the glycine-rich loop more effectively. **8** was then synthesised with a benzyl substituent which appeared to be well accommodated through molecular modelling studies. Gratifyingly, we observed significantly improved biochemical and cellular activity (0.08 μM for **8** versus 0.94 μM for **6** in pRSK MOA assay) with further improved kinase selectivity (6 versus 14 >80% inhibition at 1 μM for the same pair of compounds), albeit it with an increase in Log *D* and subsequent decrease in aqueous solubility. Compound **8** was crystallised in ERK2 where the overall binding mode was largely as predicted, the glycine-rich loop required reorganisation of Tyr-36 to fully accommodate the group (Figure 2) as commented previously. It was also notable that the angle of **8** in the ATP pocket was shifted compared to **4**. This movement of the core between the two inhibitors suggested that further work in the glycine rich loop group region might affect SAR on different parts of the scaffold which we considered in subsequent evolution of the series.

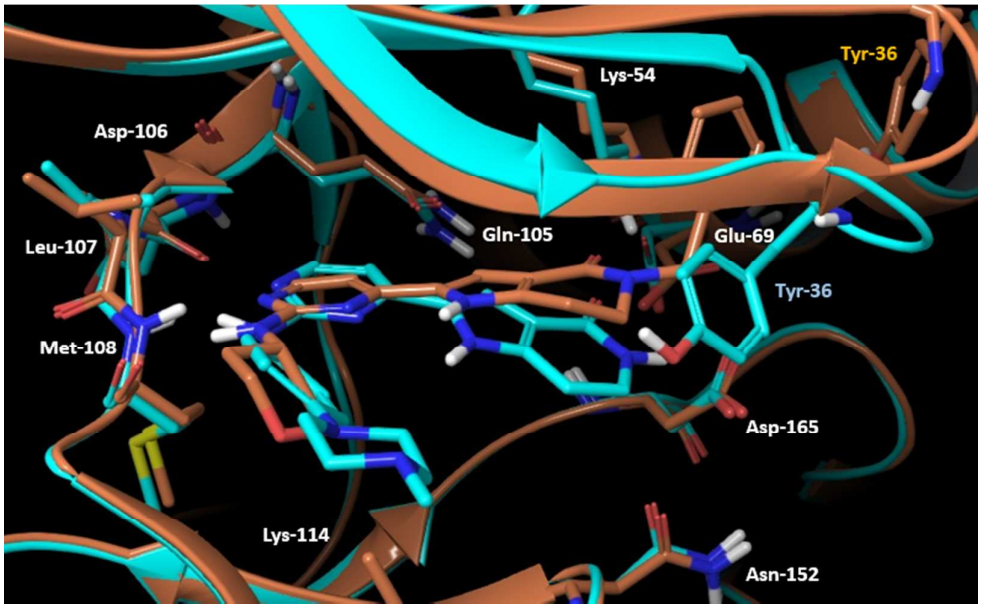

Figure 2 - Binding mode of **4** elucidated in human ERK2 crystal structure (Blue, PDB Code 5NGU) overlaid with **8** (Brown, PDB Code 5NHF).

As the lipophilicity of compounds such as **8** (Log $D_{7.4}$ 3.2) appeared to compromise physicochemical properties (aqueous solubility < 20μM), a hydroxyl group was added to the benzyl linker, using SAR gleaned from literature ERK1/2 inhibitors such as **2**, **3** and examples such as **5** by Aronov *et al*[22]. This change broadly maintained ERK activity and kinase selectivity but reduced Log *D* and resulted in improved solubility (aqueous solubility of **9** was 250 μM). In an effort to understand if the more specific reported phenyl glycine-rich loop SAR transferred to our template, **10** and **11** were synthesised with the 3-Cl, 4-F benzyl group amongst others, in both enantiomeric forms. **10** was the most potent example synthesised but we were concerned about the impact of high lipophilicity (Log $D_{7.4}$ 3.6) on solubility and other properties such a metabolic clearance, which was high in human liver microsomes (HLM), with a value of 73 μL min^{-1} mg^{-1}. An additional concern was that although the intrinsic permeability of **9** appeared acceptable in a CaCo2 assay with efflux inhibitors (A to B Papp 12 x 10^{-6} cm/s) we measured an efflux ratio of 24 in our CaCo2 efflux assay which may limit oral bioavailability. It was suspected that the additional hydroxyl group, which had successfully reduced the Log *D* of the molecules, might contribute significantly to this liability. The profile of these more potent compounds appeared to show they were primarily inhibitors of catalysis (IOC), i.e. ATP competitive inhibitors of ERK1/2 catalytic activity, due to their greater activity against pRSK than pERK in the cellular assays.

Optimisation of pyrimidine-pyrrololactam series. One focus of this early work was to identify substituents which could interact in the glycine-rich loop region of ERK1/2 but have lower lipophilicity to give a more balanced overall compound profile. In particular, such a change might enable the reduction of the Log *D* of compounds within this scaffold without the need for the hydroxyl group which may compromise permeability and or efflux. A diverse set of compounds was synthesised to vary this position and **12** and **13** appeared most interesting (table 3), having a reasonable balance of ERK2 inhibition and lipophilicity, quantified by cell lipophilicity ligand efficiency (cellular LLE). The cellular LLE was derived by subtracting the measured Log *D* from the pIC_{50} in the pRSK cellular assay. The cellular LLE for **8** (3.4) was used as a benchmark for this work, it was therefore encouraging to see compounds with increased LLE come from this compound set. Figure **3** shows the binding mode for **12**, with the CH_2CH_2-OMe group directed into the space previously occupied by the benzyl moiety. Water molecules were observed in the glycine-rich loop pocket with this group bound (but not

with the benzyl group) suggesting the pocket was not filled as fully by this group. However, kinase selectivity was not only maintained, but on occasions improved with these alternative glycine-rich loop interacting groups.

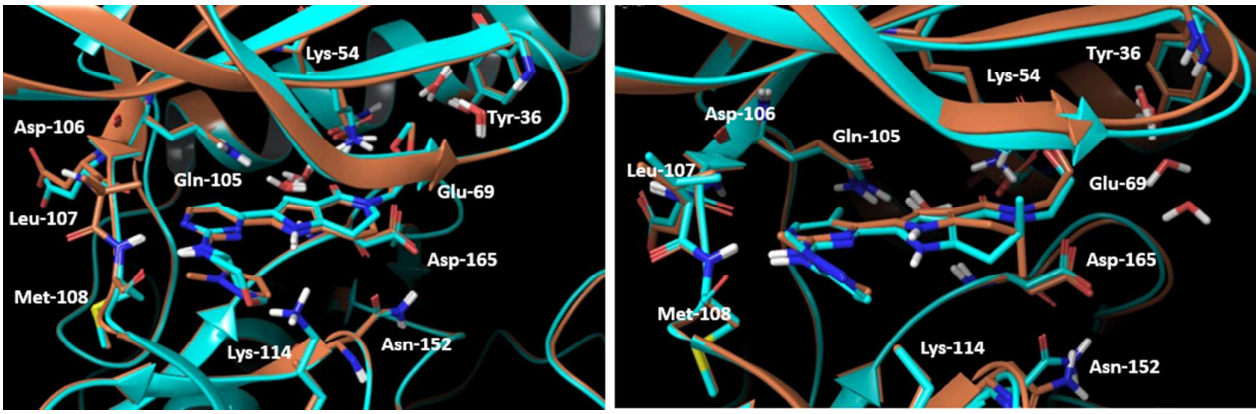

Figure 3 - Binding mode of **12** elucidated in human ERK2 crystal structure (Left blue, PDB Code 5NHH) overlaid with **14** (Left brown, PDB Code 5NHJ) and **17** (Right blue, PDB Code 5NHL) overlaid with **18** (Right brown, PDB Code 5NHO).

These structural changes which reduced Log *D*, as hoped, reduced *in vitro* clearance although these were still relatively high in HLM. Cross species *in vitro* metabolite identification work in hepatocytes had previously led us to identify the THP group as a metabolic liability, consistent with recent reports in the literature by Blake *et al* and others[13,18,25]. From this observation **14** was synthesised, containing a pyrazole group which appeared to mitigate some of these liabilities whilst demonstrating good ERK2 activity and maintaining excellent kinase selectivity. The binding mode of this compound highlighted the nitrogen of the pyrazole had the potential to interact with Lys-114, similarly to the THP group, but this interaction was not always observed in crystal structures in examples such as **14** potentially due to the inherent flexibility of the residue. The HLM clearance was 5.1 μL min^{-1} mg^{-1} for **14** which appeared to confirm a reduced metabolic liability of compounds containing this moiety. With an aim to further improve potency, ligand bound crystal structures were analysed to identify areas around **12** and **14** where the ATP pocket could be filled more effectively. A methyl group was subsequently added, positioned adjacent to the glycine rich loop substituent. Synthesised initially as a racemate, the compound was isolated and tentatively assigned chirality by VCD (Experimental S2), **15** appeared more potent than **16** in the biochemical assays (<0.00033 vs 0.014 μM at high ATP). However, there was no clear separation in activity in the MOA cellular assay (1.2 v 1.1 μM in pRSK), these changes however did improve solubility and lead to compounds with low *in vitro* clearances. At this stage we decided to continue to assess the activity of both enantiomers and assign the chirality on key compounds only where further studies were

justified. A further change was made by adding a methyl to the 5-position of the pyrimidine to fill the space towards the gatekeeper residue (Gln-105) more optimally. Both **17** and **18** showed potent biochemical and cellular activity (0.2 and 0.13 μM in pRSK respectively) and although kinase selectivity appeared slightly reduced the compounds were significantly more potent therefore the absolute margin to some of those kinase targets may well be maintained. The additional methyl directed towards the gatekeeper residue appeared to be accommodated with little impact on the binding mode of the scaffold (Figure 3). Although we did not attempt to assign absolute chirality to this pair using VCD, this was revealed through x-ray crystallography. The binding mode of **17** and **18** showed that the glycine rich loop group was maintained in a similar position, again with water observed in the pocket, the chiral methyl pointed 'up' (**17**) or 'down' (**18**) and the lactam ring puckered to enable the appropriate geometry leaving the hinge interaction largely unchanged. An interesting observation within this set was that **18** had increased activity against pERK (0.03 μM) which was not observed with closely related examples. It was also apparent that different glycine rich loop groups may have a different preference for the chirality of this adjacent methyl so we routinely synthesised both.

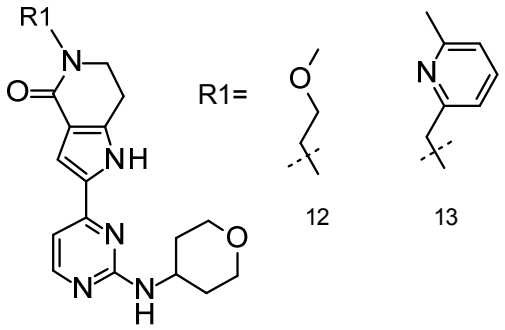

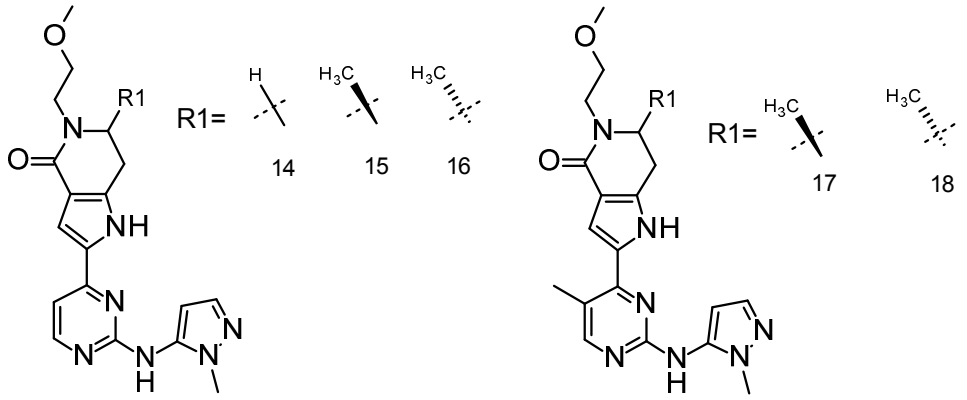

	12	13	14	15	16	17	18
ERK2 Biochemical, k_M ATP IC_{50} (μM)	<0.00113	0.00047	0.00539	<0.0003	0.0019	<0.0003	<0.0003
ERK2 Biochemical, High ATP IC_{50} (μM)	0.0048	0.001	0.0025	<0.00033	0.014	<0.0003	<0.0003
Cell MOA A375 pERK/pRSK IC_{50} (μM)	18/0.6	9.4/0.37	>30/1.6	1.1/29	1.2/11.7	8.1/0.2	0.03/0.13
Cell LLE (pRSK)	4.6	4	4.3	4.1	4.1	4.4	4.8
Log $D_{7.4}$[a]	1.6	2.4	1.4	1.8	1.7	2.11	2.14
Aqueous Solubility (μM)[b]	>370	7.2	66	627	619	>1000	>774
Kinase Selectivity (N>80% out of 128 Kinase panel)	2	2	2	2	ND	ND	6
In-vitro Clearance HLM, (Rat Heps)[c]	9.8 (3)	24 (2.8)	5.1 (7.3)	<3 (<1)	6.3 (2.2)	26 (8.9)	<4.6 (<1.5)
CaCo2 Efflux Ratio	10.2	19.6	43.5	41	33.4	ND	11.2

Table 3 – Exemplar compounds from the pyrimidine-pyrrololactam series. All IC_{50} data are reported as μM and are the mean of at least n=3 independent measurements. [a]Distribution coefficient between 1-octanol and aqueous phosphate buffer at pH 7.4. [b]Solubility of compounds in aqueous phosphate buffer at pH 7.4 after 24 h at 25 °C (μM). Kinase selectivity data measured at 1 μM compound concentration. [c]Human microsome (μL min^{-1} mg^{-1}) and rat hepatocytes metabolism intrinsic clearance (μL min^{-1} million $cells^{-1}$). ND, not determined.

Although these modifications successfully improved potency and reduced *in vitro* clearance, efflux was still a potential concern. The compounds in table 3 highlight this with efflux ratios of between 10 and 44. Examples from this series were tested in *in vivo* pharmacokinetic studies (PK) where low oral bioavailability was observed in rat, and high *in vivo* clearance in rat and mouse. However, increased compound exposure could be observed at higher doses in rat, suggesting saturation of efflux transporters might be possible. Furthermore, increased exposures could also be achieved in mouse via co-dosing with 1-aminobenzotriazole (ABT), an irreversible inhibitor of cytochrome P450's, to reduce the metabolic component of the high *in vivo* clearance. With these issues in mind, we decided to further optimise the PK properties to identify a compound with the potential to modulate the target *in vivo*, at low doses, without the need for co-dosing with ABT, as this would complicate and compromise further studies such as xenograft efficacy experiments, in particular with respect to potential combination studies with other inhibitors of the pathway.

Core change of pyrimidine-pyrrololactam series. To improve the PK properties of our compounds we aimed to either modify or replace the pyrrololactam group, as the hydrogen bond donor of the pyrrole was a concern in terms of efflux and or permeability. The methylation of the NH was well tolerated with exemplar **19** (0.0014 μM vs 0.0012 μM for **6**) and that encouraged us to make additional examples with extended glycine-rich loop groups, reassuringly the CaCo2 efflux ratios of such compounds were significantly reduced (Table 4).

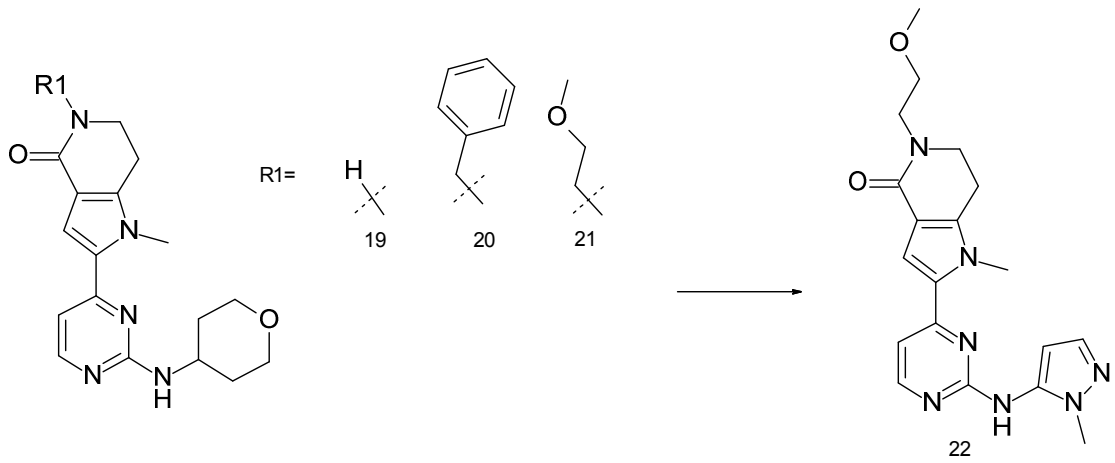

	6	19	20	21	22
ERK2 Biochemical, k_M ATP IC_{50} (μM)	0.0012	0.0014	<0.00048	0.0027	0.023
ERK2 Biochemical, High ATP IC_{50} (μM)	0.0092	0.0079	0.0016	0.024	0.24
Cell MOA A375 pERK/pRSK IC_{50} (μM)	0.96/0.94	0.57/0.34	9.3/0.069	24/1.4	>10/4.7
Log $D_{7.4}$[a]	1.3	1.3	3.3	1.7	ND
Aqueous Solubility (μM)[b]	760	410	2	82	ND
Kinase Selectivity (N>80% out of 128 Kinase panel)	14	2	ND	ND	ND
In-vitro Clearance HLM, (Rat Heps)[c]	<3 (<1)	<3 (<1.6)	84 (39)	11 (6.6)	ND
CaCo2 Efflux Ratio	ND	7.3	0.7	1.1	6.9

Table 4 – Methylation of pyrrololactam NH. All IC_{50} data are reported as μM and are the mean of at least n=3 independent measurements. IC_{50} data reported as <0.0003 μM refers to values below the tight binding limit of the ERK2 biochemical assays. [a]Distribution coefficient between 1-octanol and aqueous phosphate buffer at pH 7.4. [b]Solubility of compounds in aqueous phosphate buffer at pH 7.4 after 24 h at 25 °C (μM). Kinase selectivity data measured at 1 μM compound concentration. [c]Human microsome (μL min^{-1} mg^{-1}) and rat hepatocytes metabolism intrinsic clearance (μL min^{-1} million $cells^{-1}$). ND, not determined.

Of particular note was the improved kinase selectivity of the compound without the extended glycine rich loop group (**19**), compared to the pyrrololactam matched pair **6**. As previously observed we saw increased potency

with the addition of the benzyl into the glycine rich loop pocket (0.069 for **20** v 0.34 μM for **19** in pRSK), the CH_2CH_2OMe equivalent however was significantly less potent on this core (1.4 μM versus pRSK). An additional challenge was revealed when an example was synthesised with the pyrazole solvent channel group where a drop in biochemical potency was observed (0.24 for **22** v 0.024 μM for **21** at high ATP) and cellular potency (4.7 μM versus pRSK) which we subsequently rationalised by the 'clash' of the added methyl with the pyrazole making the binding mode less favourable. **22** was soaked into our ERK2 structural system and the binding mode was compared to **14**. Although subtle, there is a shift of the inhibitor core which appears to be required to enable the compound to bind. In addition it is possible that the bound conformation of **22** is a higher energy conformation relative to the global minimum in solution although no attempt was made to characterise this further as the SAR clearly indicated this combination of substituents was not well tolerated by the protein.

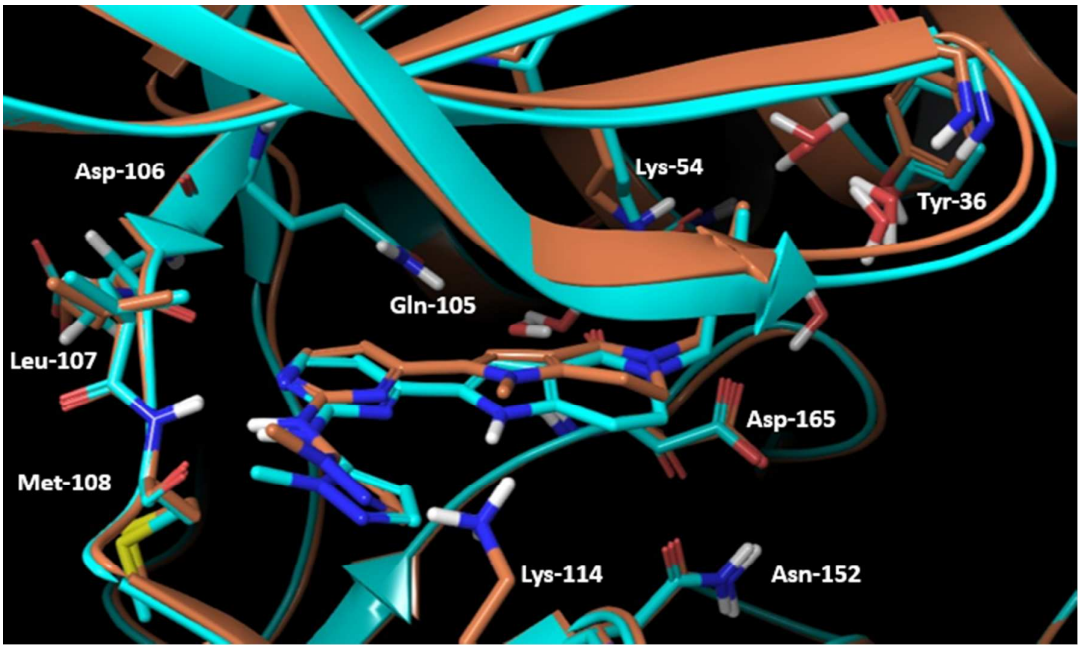

Figure 4 - Binding mode of **22** elucidated in human ERK2 crystal structure (Brown, PDB Code 5NHP) overlaid with compound **12** (Blue, PDB Code 5NHH).

Focus of this work then moved on to the identification of additional cores to access compounds with reduced efflux but which would tolerate the pyrazole solvent channel group. A number of fused ring systems were assessed based on a molecular modelling evaluation of whether the ring system could enable the appropriate binding mode geometry. These computational studies involved calculating the energetics of the bond rotation between the pyrimidine hinge group and the fused ring system by quantum mechanics (QM) to assess if the binding mode was likely to be favoured, or at least accessible without a significant energetic penalty. Selected

calculations are reported in Figure 5 which shows for the pyrrololactam systems (A and B) the binding mode as drawn is at a minimum of the torsional energetic profile (0 degrees), which was also the case for the newly identified pyrrolopyrazinone system (C).

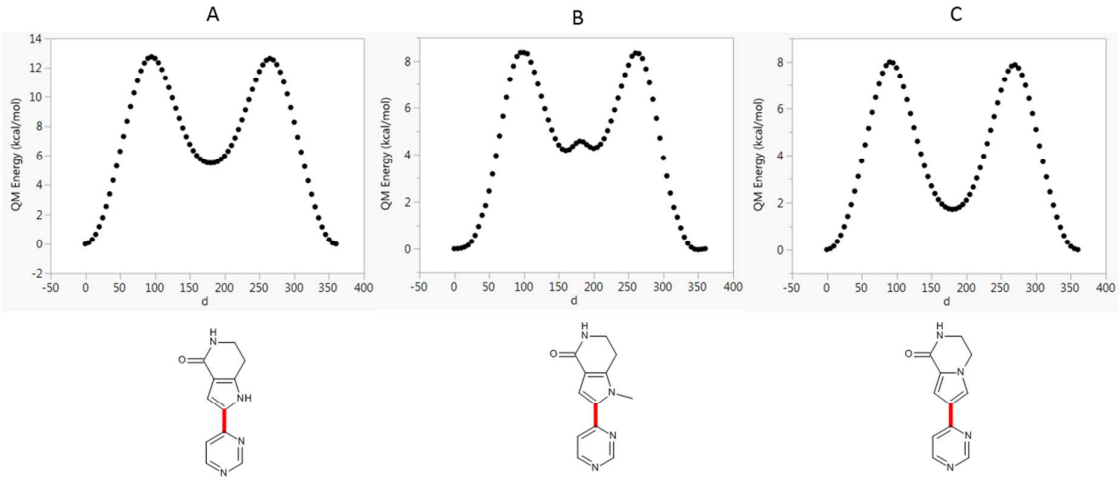

Figure 5 – QM torsion profile of an alternative pyrrolopyrazinone ring system (**C**) compared to pyrrololactam cores **A** and **B**. Gas phase energy reported in kcal/mol, calculated in Jaguar (Maestro version 2016-1, Schrodinger) using relaxed coordinate scan with an increment of 5 degrees (d), a DFT (B3LYP) and 6-31g** basis set.

In parallel likely physicochemical properties and chemical feasibility of such alternative cores was assessed. Our first example containing core **C** (**23**) showed respectable potency and kinase selectivity compared to equivalent compounds with **A** and **B** cores. Since we carried out this work, this ring system has been independently reported in ERK1/2 inhibitors by Bagdanoff *et al.*[25] from focused screening. Additional examples were then synthesised informed by mapping the previously identified SAR from the pyrrololactam cores onto a pyrrolopyrazinone scaffold, this included both solvent channel and glycine-rich loop groups along with the 'flanking' methyl's. This approach was supported by the crystal structure of **23** which showed an almost identical binding mode to the previously described pyrrololactam **14** (Figure S2, supporting information). These compounds not only showed good biochemical and cellular potency but the lipophilicity was lower than previous examples (Log *D* ~2) which gratifyingly resulted in lower *in vitro* clearances. In particular the pyridine glycine-rich loops compounds were attractive in terms of potency and properties such as solubility (Table 5). Two key compounds **24** and **25** (absolute stereochemistry unassigned) helped build confidence that the previous SAR in the glycine rich loop region reported in this manuscript could be mapped onto this alternative core (0.33 μM pRSK cell activity for **24**).

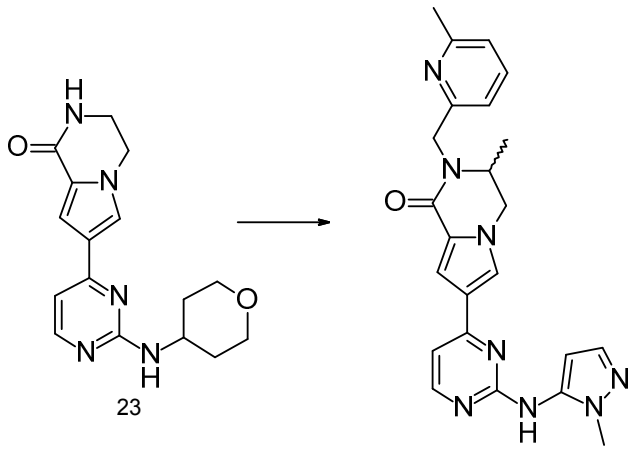

23 24 and 25

	23	24	25
ERK2 Biochemical, k_M ATP IC_{50} (μM)	0.0028	<0.00039	0.0029
ERK2 Biochemical, High ATP IC_{50} (μM)	0.037	0.00035	0.016
Cell MOA A375 pERK/pRSK IC_{50} (μM)	25/1.1	22/0.33	>30/0.73
Log $D_{7.4}$[a]	0.75	2.3	2.3
Aqueous Solubility (μM)[b]	770	560	710
Kinase Selectivity (N>80% out of 128 Kinase panel)	7	ND	ND
In-vitro Clearance HLM, (Rat Heps)[c]	<3 (<1)	8.9 (2.7)	<3 (6.4)
CaCo2 Efflux Ratio	10.4	3	4.8

Table 5 – Pyrrolopyrazinone series data. All IC_{50} data are reported as μM and are the mean of at least n=3 independent measurements. IC_{50} data reported as <0.0003 μM refers to values below the tight binding limit of the ERK2 biochemical assays. [a]Distribution coefficient between 1-octanol and aqueous phosphate buffer at pH 7.4. [b]Solubility of compounds in aqueous phosphate buffer at pH 7.4 after 24 h at 25 °C (μM). Kinase selectivity data measured at 1 μM compound concentration. [c]Human microsome (μL min^{-1} mg^{-1}) and rat hepatocytes metabolism intrinsic clearance (μL min^{-1} million $cells^{-1}$). ND, not determined.

The change in core also enabled compounds to be identified with lower efflux ratios, along with high intrinsic permeability (**25** CaCo2 A to B Papp 50 $x10^{-6}$ cm/s). A further iteration of compounds was then synthesised to include the 5-substituent pyrimidine SAR previously identified which lead to a number of key examples for further assessment and the most interesting examples from this work to date (Table 6). **26-29**, **35** and **36** were highly potent and in a Log *D* range where we expected good solubility. With potencies generally approaching (or at) the tight binding limit of the biochemical assays, the cellular activity of these compounds became the key driver in terms of compound assessment. The cellular pRSK assay identified **35** as particularly potent and it benefitted from good *in vitro* properties, including excellent aqueous solubility (>480 μM), low in-vitro clearance (<1 μL min^{-1} million $cells^{-1}$ in human heps) along with good permeability (52 x 10^{-6} cm/s) and moderate CaCo2 efflux ratio (9.6). The cellular MOA A375 pERK/pRSK potency of **35** (0.012/0.062 μM) was lower than of **1** (0.004/0.02 μM) but compared favourably to **2** and **3** in the same assays (4.1/0.14 μM and 0.031/0.086 μM respectively). The kinase selectivity was also favourable and consistent with previous examples, the profile of **35** is shown across a 288 kinase panel in Table S1, supporting information. As we expected these compounds to have highly desirable profiles both enantiomers were synthesised to enable full characterisation and profiling. There was also, on occasions, an impact of chirality on the apparent mechanism of action (MOA) which we were unable to explain, with **29** and **35** appearing to inhibit pERK to a greater extent than compounds previously synthesised within this template, consistent with a dual inhibition of catalysis (IOC) and prevention of activation (POA) profile. A profile which prevents the activation of ERK1/2 may arise from an inhibitor binding to the protein in a conformation which precludes the binding of MEK. These data suggests that varying interactions between ligand and protein in the glycine rich loop region might be able to influence the mechanistic profile of ERK1/2 small molecule inhibitors, additional studies to understand this would be valuable.

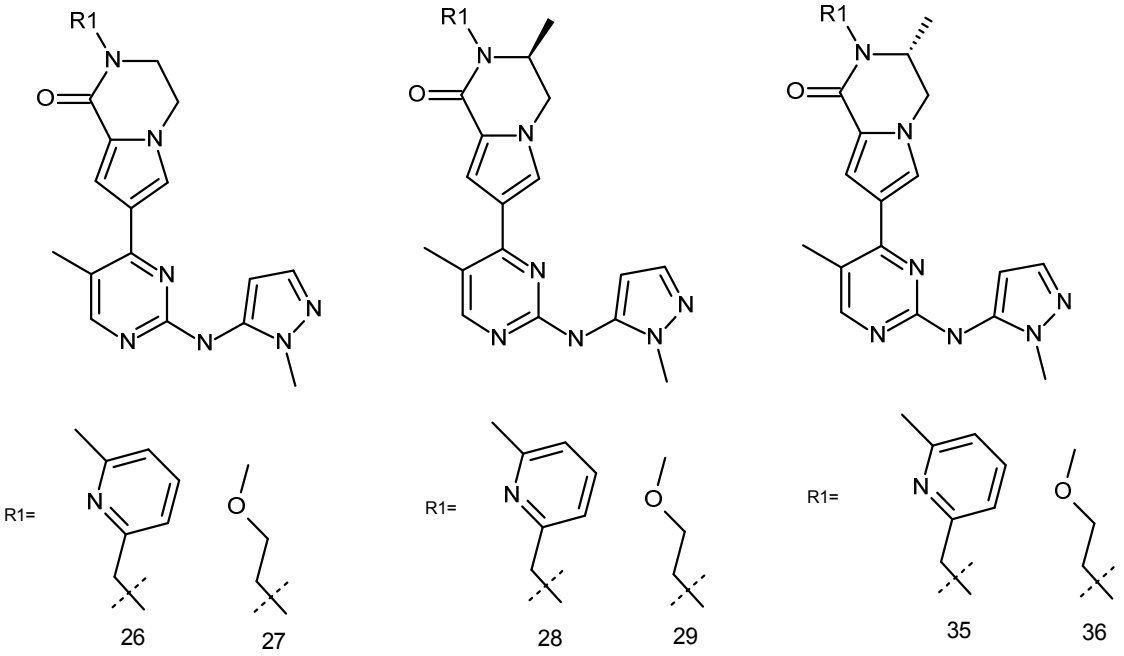

	26	**27**	**28**	**29**	**35**	**36**
ERK2 Biochemical, k_M ATP IC_{50} (μM)	<0.0003	<0.0003	<0.0003	<0.0003	<0.0003	<0.0003
ERK2 Biochemical, High ATP IC_{50} (μM)	0.0003	<0.0003	0.0009	<0.0003	0.0005	0.0002
Cell MOA A375 pERK/pRSK IC_{50} (μM)	>1/0.11	>30/0.31	>30/0.14	0.38/0.31	0.012/0.062	22/0.13
Log $D_{7.4}$[a]	2.2	1.3	2.4	1.6	2.5	1.7
Aqueous Solubility (μM)[b]	360	690	350	750	>480	620
Kinase Selectivity (N>80% out of 128 Kinase panel)	2	ND	5	8	9*	ND
In-vitro Clearance HLM, (Human/Rat Heps)[c]	<3.5 (1.8)	<3 (16)	<3 (8.9)	<3 (1.5)	<4.8 (<1/17)	5.7 (5)
CaCo2 A to B Papp + inhibitors (10^{-6} cm/s)	39	ND	34	36	52	33
CaCo2 Efflux Ratio	17	ND	11.6	11.8	9.6	7.8

Table 6 – Summary table of best combinations on pyrrolopyrazinone core. All IC_{50} data are reported as μM and are the mean of at least n=3 independent measurements. IC_{50} data reported as <0.0003 μM refers to values below the tight binding

limit of the ERK2 biochemical assays. [a]Distribution coefficient between 1-octanol and aqueous phosphate buffer at pH 7.4. [b]Solubility of compounds in aqueous phosphate buffer at pH 7.4 after 24 h at 25 °C (μM). Kinase selectivity data measured at 1 μM compound concentration, [*]tested in a broader set of 288 kinases. [c]Human microsome (μL min^{-1} $mg^{-1)}$, human and rat hepatocytes metabolism intrinsic clearance (μL min^{-1} million $cells^{-1}$). ND, not determined.

Chemistry

Synthesis of **35** was performed in a 6-step sequence as shown in Scheme 1. Starting from 1-BOC-2-(methoxycarbonyl)pyrrole-4-boronic acid pinacol ester, a Suzuki-Miyaura cross-coupling reaction with 2,4-dichloro-5-methylpyrimidine, followed by deprotection afforded pyrrole **31**. Reaction of the pyrrole with a BOC-sulfamidate followed by subsequent deprotection resulted in spontaneous lactam formation under basic conditions to deliver dihydropyrrolopyrazinone **33**. Deprotonation of the lactam followed by alkylation with 2-(chloromethyl)-6-methylpyridine yielded tertiary lactam **34**. Finally, the 1-methyl-*1H*-pyrazol-5-amino moiety was introduced by Buchwald-Hartwig cross-coupling using BrettPhos 3rd generation pre-catalyst to afford **35** in good yield. Full compound synthesis experimental details and characterisation for **35** can be found in the experimental section, and all final compounds detailed can be found in supplementary material experimental S1.

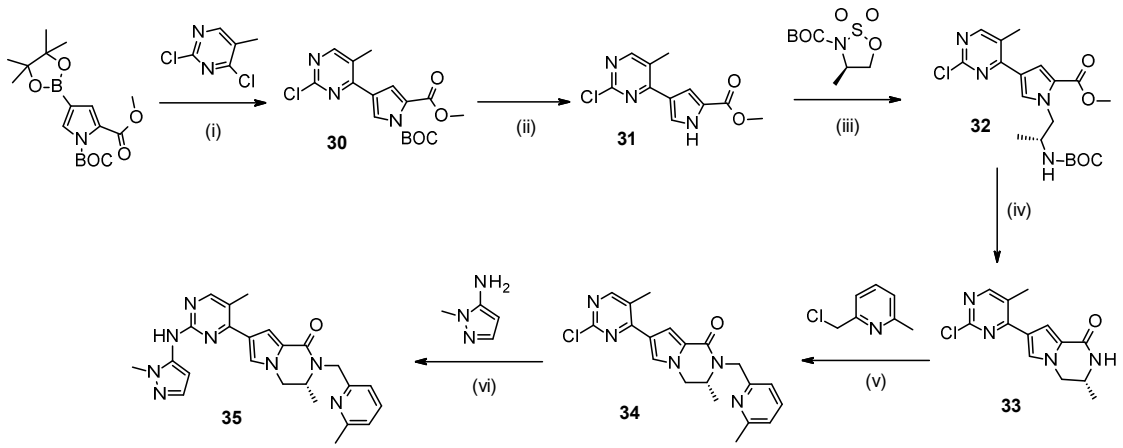

Scheme 1 – Synthesis of **35**[a]

[a]Reagents and conditions: (i) $Pd(PPh_3)_4$, K_3PO_4, 1,4-dioxane, water, 80°C, 64%; (ii) HCl, 1,4-dioxane, MeOH, 99%; (iii) K_2CO_3, 18-Crown-6, 1,4-dioxane, 100°C, 93%; (iv) trifluoroacetic acid, CH_2Cl_2, 22°C then NH_3, MeOH, 22°C, 95%; (v) NaH, DMF, 20 °C, 83%; (vi) 3G BrettPhos pre-catalyst, Cs_2CO_3, *tert*-BuOH, 80°C, 77%.

Pharmacokinetic (PK) studies on lead compound 35

Based on overall properties **35** was selected for further assessment of its potential in *in vivo* target modulation studies. **35** subsequently showed excellent *in vivo* PK properties in mouse, rat and dog studies confirming its suitability as an *in vivo* ERK1/2 inhibitor (Figure 6). Oral bioavailability in rat was measured at 31%, with 87% bioavailability in dog. A 100 mg/Kg oral dose in mouse gave free cover over the cellular pRSK IC_{50} for around 18 h (Figure 6). To understand the potential of this compound as an advanced candidate we calculated a predicted dose to man of between 91 to 251 mgs using scaled human hepatocyte data, correcting volume estimates for protein binding differences from preclinical species and requiring free cover for 12 h over pRSK IC_{50}, summarised in figure 6 with predicted human PK parameters.[26] The extent and duration of cover was chosen based on coverage required to observe tumour regression in the Calu-6 *in vivo* model.

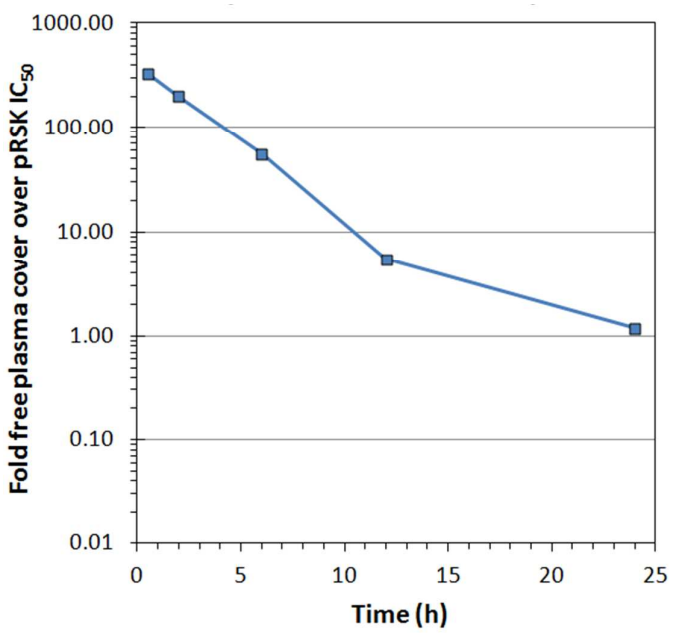

	35
Plasma protein binding % unbound (Human/Rat)	12.7 / 24.9
Rat plasma PK CL (mL/min/kg) / V_{ss} (L/kg)/ F_{oral} (%)	32 / 1.3 / 31
Dog plasma PK CL (mL/min/kg)/ V_{ss} (L/g)/ F_{oral} (%)	8 / 0.9 / 87
Predicted dose to man	91-251 mgs
Predicted human PK Cl (mL/min/kg)/ V_{ss}(L/kg)/ F_{oral} (%)	2.0/ 0.4-0.7/ 90

Figure 6 - Free plasma concentrations in nude mice following 100 mg/Kg daily oral dose of **35** in relation to cover over pRSK IC_{50} (left). PK properties and early dose to man predictions for **35** (right).

Pharmacodynamic (PD) and efficacy studies on lead compound 35

In vivo PD evaluation and antitumor xenograft studies were subsequently carried out in the Calu-6 non-small cell lung cancer (NSCLC) model. It has been widely reported the KRAS mutant cell lines can be both sensitive

and insensitive *in vitro* to inhibition of the MAPK pathway inhibition[27]. The NSCLC Calu-6 cell line possess a mutation in the KRAS gene (Q61H) and has been demonstrated to be sensitive *in vitro* to MEK inhibition, and Calu-6 xenografts were strongly growth inhibited by the allosteric MEK inhibitor selumetinib[28]. Based on this known response to *in vitro* and *in vivo* to MAPK pathway inhibition the Calu-6 cell line was selected as a relevant model for this study.

Gratifyingly, an increase in free plasma concentrations of **35** was observed in animals tested with an increasing dose of 10, 30 and 100 mg/kg, this was coupled with an overall decrease in levels of pRSK (phospho-p90RSK) a downstream target of ERK1/2 (Figure 7). A dose response relationship was observed when mice were tested chronically with **35** for 17 d (Figure 8). Tumour regressions were observed at both 15 and 50 mg/Kg compound doses QD, albeit transiently at the lower dose of 15 mg/Kg.

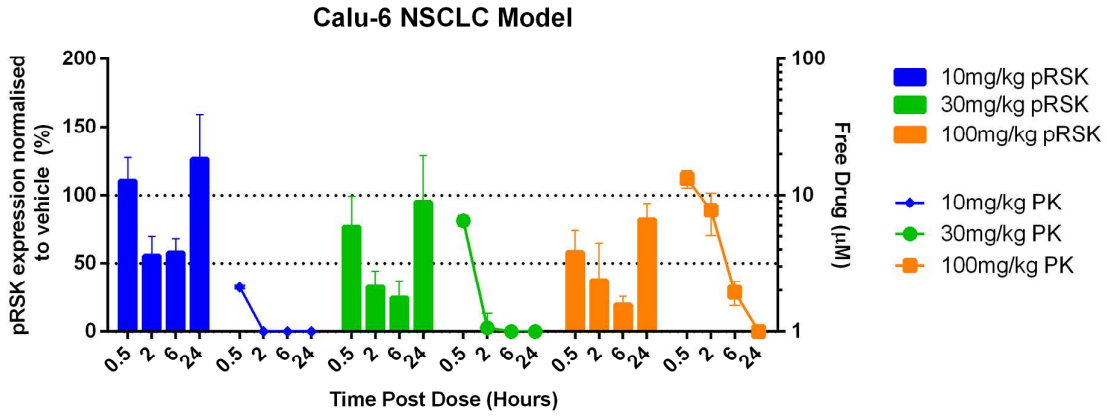

Figure 7 – Pharmacodynamic (PD) evaluation of 35 in the Calu-6 *in vivo* model of NSCLC.

Average percent pRSK expression normalised to vehicle controls over time (bar chart). PK: Average concentration of free drug over time. Error bars ± SEM (line chart).

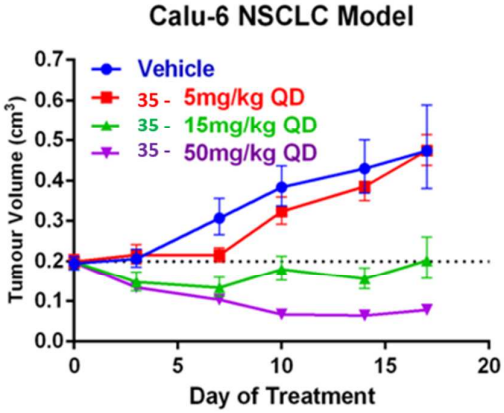

Figure 8 – Anti-tumour efficacy of 35 in the Calu-6 NSCLC model. Average tumour volume of Calu-6 over time when treated with an oral formulation of **35** at 5, 15 and 50 mg/kg. Average volumes = geomean, error bars ± SEM.

Conclusion

We have described an approach for the identification of potent and selective reversible ERK1/2 inhibitors utilising in-house kinase selectivity panel data as a start point, followed by the rapid evolution using knowledge of the compound binding mode. A number of these compounds have excellent biochemical and cellular ERK potency and are highly selective for ERK1/2 in kinase selectivity panels. An exemplar compound from this work (**35**) was dosed in a mouse antitumor study and demonstrated robust rumour regression at a 50 mg/kg daily dose. In addition, this compound had a relatively low predicted human dose (91-251 mg), showing compounds from this series justify further evaluation.[29]

Experimental

General Analytical Information

Nuclear Magnetic Resonance (NMR) spectra were recorded on a Bruker 300, 400 or 500 MHz instrument at room temperature unless otherwise stated. All ^{1}H NMR spectra were measured in part per million (ppm) relative to the signals for residual dimethyl sulfoxide (DMSO) in deuterated DMSO (2.50 ppm), or the signals for tetramethylsilane (TMS) added into the deuterated chloroform (0 ppm). Data for ^{1}H NMR were reported as: chemical shift, multiplicity (s = singlet, d = doublet, t= triplet, q = quartet, h = heptet, m = multiplet, br = broad), coupling constants, and integration. LC-MS analyses were performed on a Waters 2795 Separations Module, using a Gemini NX-C18 column, with a Waters Micromass detector. All final compounds were found to be of 95% purity or greater by LC-MS.

Synthesis and characterisation of compound 35

1-*tert*-Butyl 2-methyl 4-(2-chloro-5-methylpyrimidin-4-yl)-*1H*-pyrrole-1,2-dicarboxylate (30). Tetrakis(triphenylphosphine)palladium(0) (0.98 g, 0.85 mmol) was added to a de-gassed solution of 2,4-dichloro-5-methylpyrimidine (4.6 g, 28 mmol), 1-*tert*-butyl 2-methyl 4-(4,4,5,5-tetramethyl-1,3,2-dioxaborolan-

2-yl)-*1H*-pyrrole-1,2-dicarboxylate (10 g, 28 mmol) and potassium phosphate (18 g, 85 mmol) in dioxane (120 ml) and water (30 ml) at 22°C under nitrogen. The resulting solution was stirred at 80 °C for 4 h. The reaction mixture was concentrated and diluted with EtOAc (150 mL) and brine (100 mL). The layers were partitioned, then the aqueous layer was extracted with further EtOAc (2 x 150 mL). Combined organics were evaporated to afford crude product. The crude product was purified by flash silica chromatography, elution solvent 5–50% EtOAc in heptane. Pure fractions were evaporated to dryness to afford **30** (6.4 g, 64 %) as a white solid. ^{1}H NMR (400 MHz, DMSO) δ 1.56 (s, 9H), 2.41 – 2.47 (m, 3H), 3.83 (s, 3H), 7.39 (d, *J* = 1.9 Hz, 1H), 8.01 (d, *J* = 1.9 Hz, 1H), 8.61 (d, *J* = 0.7 Hz, 1H); *m/z*: ES$^+$ [M-BOC+H]$^+$ 252.

Methyl 4-(2-chloro-5-methylpyrimidin-4-yl)-*1H*-pyrrole-2-carboxylate (31). Hydrogen chloride, 4.0M in dioxane (45 mL, 180 mmol) was added to **30** (6.4 g, 18 mmol) in methanol (40 mL) at 22°C. The resulting mixture was stirred at 22 °C for 18 h. The white solid was collected by filtration and washed with diethyl ether. The solid was added to water (150 mL) and EtOH (20 mL) and the suspension was stirred for 30 minutes, then 2M aqueous sodium carbonate (40 mL) was added. The product was extracted with DCM (3 x 200 mL). Combined organics were concentrated to yield **31** (4.6 g, 100 %) as a white solid. ^{1}H NMR (400 MHz, DMSO) δ 2.38 – 2.45 (m, 3H), 3.81 (s, 3H), 7.39 (d, *J* = 1.7 Hz, 1H), 7.72 (d, *J* = 1.7 Hz, 1H), 8.50 (s, 1H), 12.64 (s, 1H); *m/z*: ES$^+$ [M+H]$^+$ 252.

***(R)*-Methyl 1-(2-((*tert*-butoxycarbonyl)amino)propyl)-4-(2-chloro-5-methylpyrimidin-4-yl)-*1H*-pyrrole-2-carboxylate (32).**

Potassium carbonate (40 g, 287 mmol) was added to (*R*)-*tert*-butyl 4-methyl-1,2,3-oxathiazolidine-3-carboxylate 2,2-dioxide (9.8 g, 42 mmol), **31** (8 g, 32 mmol) and 18-Crown-6 (2.1 g, 8 mmol) in 1,4-dioxane (100 mL) at 22°C under nitrogen. The resulting mixture was stirred at 100 °C for 16 h. The mixture was diluted with ethyl acetate (600 mL) and washed with water (3 x 300 mL), saturated brine (200 mL), dried ($MgSO_4$) and concentrated. The crude product was purified by flash silica chromatography, elution gradient 0 to 60% EtOAc in heptane. Pure fractions were evaporated to dryness to afford **32** (12 g, 93 %) as a white solid. ^{1}H NMR (400 MHz, DMSO) δ 1.08 (d, *J* = 6.6 Hz, 3H), 1.16 (s, 9H), 2.42 (s, 3H), 3.80 (s, 3H), 3.83 – 4.02 (m, 2H), 4.60 (dd, *J* = 3.2, 12.9 Hz, 1H), 6.77 (d, *J* = 9.0 Hz, 1H), 7.43 (s, 1H), 7.81 (s, 1H), 8.51 (s, 1H); *m/z*: ES$^+$ [M+H]$^+$ 409.

***(R)*-7-(2-Chloro-5-methylpyrimidin-4-yl)-3-methyl-3,4-dihydropyrrolo[1,2-a]pyrazin-1*(2H)*-one (33).**

Trifluoroacetic acid (30 mL) was added to **32** (7.6 g, 19 mmol) in DCM (53 mL) at 22°C. The resulting mixture was stirred at 22 °C for 2 h. The resulting solution was concentrated then purified by ion exchange chromatography. The desired product was eluted from the column using 1M ammonia/methanol solution then evaporated to dryness to afford (*R*)-methyl 1-(2-aminopropyl)-4-(2-chloro-5-methylpyrimidin-4-yl)-*1H*-pyrrole-2-carboxylate as an off white solid. This material was dissolved in DCM (50 mL) then 7M ammonia/methanol solution (100 mL) was added and the solution was stirred at ambient temperature for a further 18 h. The reaction was concentrated and the residue was triturated with ether to yield **33** (4.90 g, 95 %) as a white solid. ^{1}H NMR (400 MHz, DMSO) δ 1.20 (d, *J* = 5.9 Hz, 3H), 2.42 (s, 3H), 3.83 – 3.93 (m, 2H), 4.25 – 4.35 (m, 1H), 7.23 (d, *J* = 1.7 Hz, 1H), 7.81 (d, *J* = 1.7 Hz, 1H), 7.92 (s, 1H), 8.49 (s, 1H); *m/z*: ES$^+$ $[M+H]^+$ 277.

***(R)*-7-(2-Chloro-5-methylpyrimidin-4-yl)-3-methyl-2-((6-methylpyridin-2-yl)methyl)-3,4-dihydropyrrolo[1,2-a]pyrazin-1*(2H)*-one (34).**

Sodium hydride (60% dispersion in mineral oil) (1.1 g, 27 mmol) was added to **33** (7 g, 25 mmol) in DMF (150 mL) at 22 °C under nitrogen. The resulting suspension was stirred at RT for 30 minutes. 2-(Chloromethyl)-6-methylpyridine (3.7 g, 26 mmol) in DMF (10 mL) was added and the resulting solution was stirred at 22 °C for 18 h. The reaction mixture was diluted with ethyl acetate (400 mL) and quenched with saturated NH_4Cl (400 mL). The organic layer was washed with brine (400 mL) water (400 mL) and concentrated. A small amount of solid was observed in the final aqueous layer, which was isolated by filtration (confirmed to be pure product) then added to the crude product. The crude product was stirred in diethyl ether (150 mL) for 1 hour, then collected by filtration and dried under vacuum to yield **34** (7.9 g, 83 %) as a white solid. ^{1}H NMR (400 MHz, DMSO) δ 1.15 (d, *J* = 6.6 Hz, 3H), 2.43 (s, 3H), 2.46 (s, 3H), 3.98 (ddd, *J* = 2.4, 4.2, 6.6 Hz, 1H), 4.23 (dd, *J* = 2.3, 13.1 Hz, 1H), 4.30 (d, *J* = 16.0 Hz, 1H), 4.38 (dd, *J* = 4.3, 13.1 Hz, 1H), 5.13 (d, *J* = 16.0 Hz, 1H), 7.15 (t, *J* = 6.9 Hz, 2H), 7.28 (d, *J* = 1.7 Hz, 1H), 7.64 (t, *J* = 7.7 Hz, 1H), 7.85 (d, *J* = 1.7 Hz, 1H), 8.50 (s, 1H); *m/z*: ES$^+$ $[M+H]^+$ 382.

***(R)*-3-Methyl-7-(5-methyl-2-((1-methyl-*1H*-pyrazol-5-yl)amino)pyrimidin-4-yl)-2-((6-methylpyridin-2-yl)methyl)-3,4-dihydropyrrolo[1,2-a]pyrazin-1*(2H)*-one (35).**

34 (130 mg, 0.35 mmol), 1-methyl-*1H*-pyrazol-5-amine (37 mg, 0.38 mmol) and caesium carbonate (250 mg, 0.77 mmol) were suspended in *tert*-butanol (3 mL) and de-gassed for 5 minutes, then BrettPhos 3rd generation pre-catalyst (16 mg, 0.02 mmol) was added. The reaction was heated to 83 °C for 2 h. The reaction mixture

was diluted with EtOAc (30 mL) and washed with brine (30 mL). The aqueous layer was extracted with DCM (2 x 30 mL) then combined organics were evaporated to afford crude product. The crude product was purified by flash silica chromatography, elution gradient 0.5 to 5% MeOH in DCM. Pure fractions were evaporated to dryness to afford **35** (120 mg, 77 %) as a yellow solid. ^{1}H NMR (400 MHz, DMSO-d_6) δ 1.15 (d, J = 6.6 Hz, 3H), 2.32 (s, 3H), 2.46 (s, 3H), 3.68 (s, 3H), 3.96 (dt, J = 3.4, 6.7 Hz, 1H), 4.20 (dd, J = 2.3, 13.0 Hz, 1H), 4.29 (d, J = 15.9 Hz, 1H), 4.36 (dd, J = 4.2, 13.0 Hz, 1H), 5.13 (d, J = 16.0 Hz, 1H), 6.26 (d, J = 1.8 Hz, 1H), 7.15 (dd, J = 4.6, 7.6 Hz, 2H), 7.25 (d, J = 1.7 Hz, 1H), 7.32 (d, J = 1.9 Hz, 1H), 7.61 – 7.68 (m, 2H), 8.23 (s, 1H), 9.06 (s, 1H); ^{13}C NMR (176 MHz, DMSO-d_6) 16.8, 16.9, 23.9, 35.3, 48.7, 48.8, 51.5, 97.8, 112.3, 116.6, 118.2, 121.5, 122.8, 124.2, 126.0, 137.0, 137.1, 138.7, 156.9, 157.3, 157.5, 158.5, 158.6, 159.7; Purity 99.7% by LC-MS, *m/z*: ES$^+$ $[M+H]^+$ 443; HRMS (ES$^+$) for $C_{24}H_{27}N_8O$ (MH^+): calculated 443.23023; found 443.23032.

Animal studies

All animal work was compliant with the UK Animals (Scientific Procedures) Act, which is consistent with EU Directive 2010/63/EU. Female athymic Nude-Foxn1 nu mice (Harlan) were housed in specific pathogen free conditions in individually ventilated cages. Calu-6 non-small cell-lung cancer cells were grown in RPMI 1640 (Invitrogen) supplemented with 10% foetal calf serum and 1% L-Glutamine (Sigma Aldrich) under standard cell culture conditions. Cells were harvested and mice were injected subcutaneously with 100µl of a 1x10^6 cell suspension of Calu-6 cells in 1:1 v/v mice of Matrigel (Becton Dickinson). Tumours growth was monitored by calliper measurement and volume calculated using the following equation (3.142 x Max (Length:Width) x Min (Length:Width) x Min (Length:Width))/6000. Mice were enrolled onto study when they reached a size of 0.4cm^3 for the PK/PD experiment, and 0.2cm^3 for the efficacy experiment, both studies were appropriately statistically powered.

Pharmacodynamic (PD) and Efficacy Evaluation

To evaluate the acute pharmocodynamic effect of **35** animals were dosed orally with the compound formulated in 10% DMSO & 90% of a 40% Kleptose solution, mice were euthanized at a range of time points after dosing, terminal blood samples were taken for mass spectrometry quantification of compound levels and tumours excised and snap frozen for Western blot analysis. Western blot was carried out as described previously[30] with

antibodies again phospho-p90RSK (Abcam). For the efficacy study mice were dosed for 17 days and tumour volumes measured twice weekly. The geomean (average of log10 volumes) of each group was calculated and plotted using GraphPad Prism 6 for windows (Graph Pad Software Inc).

Biochemical and Cellular Assays

A full description of compound handling and experimental methods for all biochemical and cellular assays referred to can be found in our previous publication[18].

ERK2 Protein Crystal Structures

Protein crystals were generated using the hanging drop technique by mixing equal volumes of protein solution (approx. 10mg/ml human Erk2 in 20mM HEPES pH7.8, 200mM NaCl, 0.5mM TCEP) and crystallisation buffer (30% PegMME2K, 100mM HEPES pH 7.6, 200mM Ammonium sulfate). Data collections were carried out at the Diamond Light Source and ESRF synchrotron beamlines at cryogenic temperatures, using ethylene glycol as cryoprotectant. The pipedream and autoBUSTER software packages were used to solve and refine the structures, the program Coot was used for manual building of the models. Data collection and refinement are listed below.

Compound	**4**	**8**	**12**	**14**	**17**	**18**	**22**	**23**
PDB Code	**5NGU**	**5NHF**	**5NHH**	**5NHJ**	**5NHL**	**5NHO**	**5NHP**	**5NHV**
Data collection statistics‡								
Space group and cell	$P2_1$	$P2_1$	$P2_1$	$P2_1$	$P2_1$	$P2_1$	$P2_1$	$P2_1$
a [Å]	49.01	49.02	48.58	49.03	48.91	48.91	48.79	48.88
b [Å]	71.14	70.05	70.49	71.16	71.34	71.80	71.11	70.60
c [Å]	60.64	60.36	61.46	61.4	61.16	61.25	61.03	60.99
β [°]	110.06	109.30	111.81	112.01	111.05	111.43	111.03	110.43
Resolution [Å]	2.75	2.14	1.94	2.12	2.07	2.24	1.99	2.00
Unique reflections	4692 (743)	20963 (1989)	28525 (2112)	21741 (1920)	23548 (1744)	18618 (1351)	26082 (3311)	25618 (8914)
Multiplicity	3.2 (3.3)	1.5 (1.4)	3.2 (3.2)	3.3 (3.2)	3.1 (3.2)	3.2 (3.2)	3.3 (3.3)	3.4 (3.4)

Completeness [%]	97.3 (97.9)	98.2 (96.4)	99.2 (99.6)	97.7 (87.8)	98.1 (98.9)	97.7 (97.7)	97.8 (96.9)	97.4 (97.1)
R_{sym} [%]	0.141 (0.537)	0.081 (0.792)	0.05 (0.520)	0.077 (0.723)	0.075 (0.340)	0.058 (0.612)	0.068 (0.357)	0.072 (0.368)
Mean(I)/sd	6.6 (1.9)	9.5 (1.6)	14.8 (2.1)	10.6 (1.5)	8.3 (2.7)	10.9 (1.7)	11.5 (3.7)	11.2 (3.5)
Refinement statistics								
# of reflections (working /test)	10077/485	20940/1312	28506/1775	21753/1108	23532/1475	18601/1166	26063/1651	25601/1596
R/R_{free} [%]	26.46/26.41	24.8/25.9	18.3/22.0	20.1/20.7	21.1/23.7	20.1/23.1	19.9/22.1	18.6/22.8
Deviation from ideal geometry								
bond lengths [Å]	0.010	0.010	0.010	0.007	0.007	0.009	0.006	0.010
bond angles [◦]	1.100	1.22	1.00	1.00	0.97	1.08	0.93	1.00
Ramachandran plot [%]								
preferred region	97.0	97.0	95.3	96.8	96.2	95.6	96.1	97.0
generously allowed	2.7	3.0	4.1	3.2	3.8	4.4	3.9	2.7
region	0.3	0	0.6	0	0	0	0	0.3
disallowed region								

‡ Data in parentheses refer to the highest resolution shell.

Table 6 – ERK2 protein crystal structure statistics.

Supporting Information Available: Additional data analyses, experimental information, compound molecular formula strings and compound characterisation can be found in the supporting information. This material is available free of charge via the Internet at http://pubs.acs.org.

Acknowledgements

We would like to thank all colleagues at AstraZeneca who were involved in the work reported in this manuscript. This includes all project team members and functions including compound purification, compound handling and technical support from the *in vivo* sciences group Alderley Park, UK (in particular Joanne Wilson, Richard Grant and Aaron Smith).

Abbreviations

ABT (1-aminobenzotriazole), HTS (high throughput screening), IOC (inhibition of catalysis), PD (pharmacodynamic), PK (pharmacokinetics), LLE (ligand lipophilicity efficiency), MOA (mechanism of action), POA (prevention of activation), THP (tetrahydropyran).

Author Information

Corresponding author:

Email: richard.a.ward@astrazeneca.com.

References

1. Dhillon, A. S.; Hagan, S.; Rath, O.; Kolch, W. MAP kinase signalling pathways in cancer. *Oncogene* **2007**, *26,* 3279-3290.

2. Hanahan, D.; Weinberg, R. A. Hallmarks of cancer: the next generation. *Cell* **2011**, *144,* 646-674.

3. Yoon, S.; Seger, R. The extracellular signal-regulated kinase: multiple substrates regulate diverse cellular functions. *Growth Factors* **2006**, *24,* 21-44.

4. Owens, D. M.; Keyse, S. M. Differential regulation of MAP kinase signalling by dual-specificity protein phosphatases. *Oncogene* **2007**, *26,* 3203-3213.

5. Vakiani, E.; Solit, D. B. KRAS and BRAF: drug targets and predictive biomarkers. *J. Pathol.* **2011**, *223,* 219-229.

6. Solit, D. B.; Garraway, L. A.; Pratilas, C. A.; Sawai, A.; Getz, G.; Basso, A.; Ye, Q.; Lobo, J. M.; She, Y.; Osman, I.; Golub, T. R.; Sebolt-Leopold, J.; Sellers, W. R.; Rosen, N. BRAF mutation predicts sensitivity to MEK inhibition. *Nature* **2006**, *439,* 358-362.

7. Flaherty, K. T.; Puzanov, I.; Kim, K. B.; Ribas, A.; McArthur, G. A.; Sosman, J. A.; O'Dwyer, P. J.; Lee, R. J.; Grippo, J. F.; Nolop, K.; Chapman, P. B. Inhibition of mutated, activated BRAF in metastatic melanoma. *N. Engl. J. Med.* **2010**, *363,* 809-819.

8. Ji, Z.; Flaherty, K. T.; Tsao, H. Targeting the RAS pathway in melanoma. *Trends Mol. Med.* **2012**, *18,* 27-35.

9. Flaherty, K. T.; Infante, J. R.; Daud, A.; Gonzalez, R.; Kefford, R. F.; Sosman, J.; Hamid, O.; Schuchter, L.; Cebon, J.; Ibrahim, N.; Kudchadkar, R.; Burris, H. A.,3rd; Falchook, G.; Algazi, A.; Lewis, K.; Long, G. V.; Puzanov, I.; Lebowitz, P.; Singh, A.; Little, S.; Sun, P.; Allred, A.; Ouellet, D.; Kim, K. B.; Patel, K.; Weber, J. Combined BRAF and MEK inhibition in melanoma with BRAF V600 mutations. *N. Engl. J. Med.* **2012**, *367,* 1694-1703.

10. Flaherty, K. T.; Robert, C.; Hersey, P.; Nathan, P.; Garbe, C.; Milhem, M.; Demidov, L. V.; Hassel, J. C.; Rutkowski, P.; Mohr, P.; Dummer, R.; Trefzer, U.; Larkin, J. M.; Utikal, J.; Dreno, B.; Nyakas, M.; Middleton, M. R.; Becker, J. C.; Casey, M.; Sherman, L. J.; Wu, F. S.; Ouellet, D.; Martin, A. M.; Patel, K.; Schadendorf, D.; METRIC Study Group Improved survival with MEK inhibition in BRAF-mutated melanoma. *N. Engl. J. Med.* **2012**, *367,* 107-114.

11. Morris, E. J.; Jha, S.; Restaino, C. R.; Dayananth, P.; Zhu, H.; Cooper, A.; Carr, D.; Deng, Y.; Jin, W.; Black, S.; Long, B.; Liu, J.; Dinunzio, E.; Windsor, W.; Zhang, R.; Zhao, S.; Angagaw, M. H.; Pinheiro, E. M.; Desai, J.; Xiao, L.; Shipps, G.; Hruza, A.; Wang, J.; Kelly, J.; Paliwal, S.; Gao, X.; Babu, B. S.; Zhu, L.; Daublain, P.; Zhang, L.; Lutterbach, B. A.; Pelletier, M. R.; Philippar, U.; Siliphaivanh, P.; Witter, D.; Kirschmeier, P.; Bishop, W. R.; Hicklin, D.; Gilliland, D. G.; Jayaraman, L.; Zawel, L.; Fawell, S.; Samatar, A. A. Discovery of a novel ERK inhibitor with activity in models of acquired resistance to BRAF and MEK inhibitors. *Cancer. Discov.* **2013**, *3,* 742-750.

12. BioMed Valley Discoveries BVD-523. *http://biomed-valley.com/portfolio/bvd-523* (accessed March 9, 2017).

13. Blake, J. F.; Burkard, M.; Chan, J.; Chen, H.; Chou, K. J.; Diaz, D.; Dudley, D. A.; Gaudino, J. J.; Gould, S. E.; Grina, J.; Hunsaker, T.; Liu, L.; Martinson, M.; Moreno, D.; Mueller, L.; Orr, C.; Pacheco, P.; Qin, A.; Rasor, K.; Ren, L.; Robarge, K.; Shahidi-Latham, S.; Stults, J.; Sullivan, F.; Wang, W.; Yin, J.; Zhou, A.; Belvin, M.; Merchant, M.; Moffat, J.; Schwarz, J. B. Discovery of (S)-1-(1-(4-Chloro-3-fluorophenyl)-2-hydroxyethyl)-4-(2-((1-methyl-1H-pyrazol-5-y l)amino)pyrimidin-4-yl)pyridin-2(1H)-one (GDC-0994), an extracellular signal-regulated kinase 1/2 (ERK1/2) inhibitor in early clinical development. *J. Med. Chem.* **2016**, *59,* 5650-5660.

14. CC-9003. *https://clinicaltrials.gov/ct2/show/NCT02313012* (accessed March 9, 2017).

15. LTT-462. *https://clinicaltrials.gov/ct2/show/NCT02711345* (accessed March 9, 2017).

16. KO-947. *https://clinicaltrials.gov/ct2/show/NCT03051035* (accessed March 9, 2017).

17. LY3214996. *https://clinicaltrials.gov/ct2/show/NCT02857270* (accessed March 9, 2017).

18. Ward, R. A.; Colclough, N.; Challinor, M.; Debreczeni, J. E.; Eckersley, K.; Fairley, G.; Feron, L.; Flemington, V.; Graham, M. A.; Greenwood, R.; Hopcroft, P.; Howard, T. D.; James, M.; Jones, C. D.; Jones, C. R.; Renshaw, J.; Roberts, K.; Snow, L.; Tonge, M.; Yeung, K. Structure-guided design of highly selective and potent covalent inhibitors of ERK1/2. *J. Med. Chem.* **2015**, *58,* 4790-4801.

19. GDC-0094. https://clinicaltrials.gov/ct2/show/NCT01875705 (accessed March 9, 2017).

20. Copeland R.A. Enzymes; 2nd edition, Wiley-VCH: New York, 2000, 305-317.

21. Cheng, Y.; Prusoff, W. H. Relationship between the inhibition constant (K1) and the concentration of inhibitor which causes 50 per cent inhibition (I50) of an enzymatic reaction. *Biochem. Pharmacol.* **1973**, *22,* 3099-3108.

22. Aronov, A. M.; Tang, Q.; Martinez-Botella, G.; Bemis, G. W.; Cao, J.; Chen, G.; Ewing, N. P.; Ford, P. J.; Germann, U. A.; Green, J.; Hale, M. R.; Jacobs, M.; Janetka, J. W.; Maltais, F.; Markland, W.; Namchuk, M. N.; Nanthakumar, S.; Poondru, S.; Straub, J.; ter Haar, E.; Xie, X. Structure-guided design of potent and selective pyrimidylpyrrole inhibitors of extracellular signal-regulated kinase (ERK) using conformational control. *J. Med. Chem.* **2009**, *52,* 6362-6368.

23. Chaikuad, A.; Tacconi, E. M. C.; Zimmer, J.; Liang, Y.; Gray, N. S.; Tarsounas, M.; Knapp, S. A unique inhibitor binding site in ERK1/2 is associated with slow binding kinetics. *Nat. Chem. Biol.* **2014**, 853-860.

24. Schrodinger, M. Small-Molecule Drug Discovery Suite 2016-3, Schrödinger, LLC, New York, NY, 2016. *https://www.schrodinger.com/* (accessed March 9, 2017).

25. Bagdanoff, J. T.; Jain, R.; Han, W.; Zhu, S.; Madiera, A. M.; Lee, P. S.; Ma, X.; Poon, D. Tetrahydropyrrolo-diazepenones as inhibitors of ERK2 kinase. *Bioorg. Med. Chem. Lett.* **2015**, *25,* 3788-3792.

26. McGinnity, D. F.; Collington, J.; Austin, R. P.; Riley, R. J. Evaluation of human pharmacokinetics, therapeutic dose and exposure predictions using marketed oral drugs. *Curr. Drug Metab.* **2007**, *8,* 463-479.

27. Solit, D. B.; Garraway, L. A.; Pratilas, C.A.; Sawai, A.; Getz, G.; Basso, A.; Ye, Q.; Lobo, J. M.; She, Y.; Osman, I.; Golub, T. R.; Sebolt-Leopold, J.; Seller, W. R.; Rosen, N. BRAF mutation predicts sensitivity to MEK inhibition. *Nature* **2006**, *439*, 358–62.

28. Davies, B. R.; Logie, A.; Mckay, J. S.; Martin, P.; Steele, S.; Jenkins, R.; Cockerill, M.; Smith, P. D. AZD6244 (ARRY-142886), a potent inhibitor of mitogen activated protein kinases. *Mol Cancer Ther.* **2007**, *6*, 2209-2219.

29. Ward, R. A.; Graham, M. A.; Swallow, S.; Jones, C. D.; Substituted 3,4-dihydropyrrolo[1,2-a]pyrazin-1 (2h) -one derivatives as kinase inhibitors. PCT Int. Appl. (2016), WO2016162325A.

30. Loddick, S. A.; Ross, S. J.; Thomason, A. G.; Robinson, D. M.; Walker, G. E.; Dunkley, T. P. J.; Brave, S. R.; Broadbent, N.; Stratton, N. C.; Trueman, D.; Mouchet, E.; Shaheen, F. S.; Jacobs, V. N.; Cumberbatch, M.; Wilson, J.; Jones, R. D. O.; Bradbury, R. H.; Rabow, A.; Gaughan, L.; Womack, C.; Barry, S. T.; Robson, C. N.; Critchlow, S. E.; Wedge, S. R.; Brooks, A. N. AZD3514: A small molecule that modulates androgen receptor signaling and function in vitro and in vivo. *Mol. Cancer Ther.* **2013**, *12,* 1715-1727.

Table of Contents graphic